J Appl Electrochem (2009) 39:1369–1377
DOI 10.1007/s10800-009-9812-7

ORIGINAL PAPER

Electrocatalytic oxygen reduction on single-walled carbon nanotubes supported Pt alloys nanoparticles in acidic and alkaline conditions

Ahmad Nozad Golikand · Mehdi Asgari · Elaheh Lohrasbi · Mohammad Yari

Received: 22 October 2008 / Accepted: 26 January 2009 / Published online: 20 February 2009
© Springer Science+Business Media B.V. 2009

Abstract The objective of this study is to improve the catalytic activity of platinum by alloying with transition metal (Pd) in gas diffusion electrodes (GDEs) by oxygen reduction reaction (ORR) at cathode site and comparison of the acidic and alkaline electrolytes. The high porosity of single-walled carbon nanotubes (SWCNTs) facilitates diffusion of the reactant and facilitates interaction with the Pt surface. It is also evident that SWCNTs enhance the stability of the electrocatalyst. Functionalized SWCNTs are used as a means to facilitate the uniform deposition of Pt on the SWCNT surface. The structure of SWCNTs is nearly perfect, even after functionalization, while other types of CNTs contain a significant concentration of structural defects in their walls. So catalysts supported on SWCNTs are studied in this research.

The electrocatalytic properties of ORR were evaluated by cyclic voltammetry, polarization experiments, and chronoamperometry. The morphology and elemental composition of Pt alloys were characterized by X-ray diffraction (XRD) analysis and inductively coupled plasma atomic emission spectroscopy (ICP-AES) system. The catalytic activities of the bimetallic catalysts in GDEs have been shown to be not only dependent on the composition, but also on the nature of the electrolytes. The GDEs have shown a transition from the slow ORR kinetics in alkaline electrolyte to the fast ORR kinetics in the acidic electrolyte. The results also show that introduction of Pd as transition metal in the Pt alloys provides fast ORR kinetics in both acidic and alkaline electrolytes. The performance of GDEs with Pt–Pd alloy surfaces towards the ORR as a function of the alloy's overall composition and their behavior in acidic electrolyte was also studied. These results show that the alloy's overall composition and also the nature of the electrolytes have a large effect on the performance of GDEs for ORR.

Keywords Platinum · Alloy · Oxygen reduction reaction · Gas diffusion electrode · Alkaline electrolyte · Acid electrolyte · Carbon nanotubes

A. N. Golikand (✉) · M. Asgari
Chemistry Department, NSTRI, Tehran, Iran
e-mail: ahmadnozadgolikand@yahoo.com

A. N. Golikand · E. Lohrasbi
Corrosion Lab., Material School, NSTRI, Tehran, Iran

M. Yari
Chemistry Department, Shahre Ghods Branch, Islamic Azad University, Shahre Ghods, Iran

1 Introduction

Electrochemical reduction of oxygen (O_2) plays a significant role in fuel cells, gas sensors, and electrosynthesis of hydrogen peroxide. It has been a pivotal subject for extensive studies in view of its importance in fuel-cell applications, and in the detection of oxygen levels in areas such as biochemistry, neuroscience, and physiology [1–5].

This has been increasing interest to develop economic and robust alternatives as electrocatalysts for the ORR [6–10]. Most of the basic studies on oxygen reduction reaction (ORR) have been conducted in acidic electrolyte [8–10]. A few ORR studies in alkaline solutions have also been reported [11–15]. The situation in alkaline electrolyte is different from that in acid electrolyte. Alkaline electrolytes present many opportunities for non-Pt catalysts for the ORR. Materials that have little or no measurable activity for the ORR in acid have substantial level of activity in alkaline solution. The first technological alkaline fuel cell,

developed by the group of Bacon at the University of Cambridge in 1950s, utilized non-Pt electrodes, a Ni anode, and a lithiated NiO cathode (electrolyte was 30 wt.% aqueous KOH). At present, in the Space Shuttle's alkaline fuel cell, rapid oxygen reduction is achieved using high-surface-area gold crystallites, where metallurgical densification and loss of surface area of the gold electrocatalysts are overcome by alloying the gold with platinum. The platinum is located in the core of the binary alloy electrocatalyst particle and therefore is not directly involved in oxygen electroreduction. Although the remarkable pH effect has been known for some time, the fundamental reason is still elusive.

Platinum supported on high-surface-area carbon nanotubes shows increased catalytic activity for ORR in acidic or alkaline media. Various Pt-based alloy catalysts (binary, ternary, and quaternary alloys) have also been tested as electrocatalysts for ORR in the last two decades [14–21]. Alloy catalysts have been proposed and tested with various degrees of success, attributed to the changes in the electronic structure with respect to that of Pt and to the changes in the physical structure of the catalyst (metal–metal distances and coordination numbers). It has been demonstrated that the use of alloys such as Pt–Fe, Pt–Ni, Pt–Co, and Pt–Cr leads to enhancement in the activity of oxygen reduction on the cathode of the fuel cell compared with use of pure platinum. Bimetallic Pt alloys as oxygen reduction catalysts have also been reported [15, 17, 21–26]. Wang et al. have studied the reaction thermodynamics for direct four-electron reduction, evaluating the Gibbs free energy change for each step on a group of transition-metal atoms [27]. This shows that it is possible to separate the effect of the first reduction step from those of the last three steps, which may be considered coupled. Wang et al. [27] and Sidik et al. [28] suggested that the oxygen molecule does not dissociate before the first electron and proton transfer and that the product for this step is OOH, which dissociates on the surface. A study by Calvo et al. [29] on the change of reaction energy (at 0 K) for direct four-electron reduction evaluated ΔE_1 for the first electron reduction step on a given metal site M as:

$$O_2 + M + H^+ + e- \rightarrow M-OH \quad (1)$$

followed by ΔE_2 for the reaction:

$$M-OH + M-O + 3H^+ + 3e- \rightarrow 2M + 2H_2O, \quad (2)$$

which combines the last three electron and proton transfers representing successive reductions of the adsorbed hydroxyl and atomic oxygen—resulting from the dissociation of the OOH intermediate—to water molecules. Calvo et al. had also proposed [29] that a good ORR catalyst could be designed as the combination of a metal that adsorbs OOH more strongly than Pt, and a second metal able to bind OH and O less strongly than Pt, thus favoring O and OH reduction to water. As proposed by Yeager [30], reduction of O_2 in aqueous solutions generally proceeds by one of two pathways: one is a direct four-electron pathway through which the molecular oxygen is reduced to HO_2^-, followed by further reduction to OH^- or its direct decomposition to OH^-. Normally the second route is more likely to occur in alkaline solutions. Yeager also proposed that the electroreduction of molecular oxygen involves dissociative absorption of O_2 by a strong interaction between metal and oxygen and a redox reaction of the catalyst site. Transition metals, due to their ability to form chemical bonds with O_2 through their *d* orbitals, have been investigated as non-noble-metal electrocatalysts for oxygen reduction [31–34]. The mechanism of ORR in alkaline medium is not clearly known. Although it is suggested that ORR in alkaline media proceeds by a multistep mechanism involving adsorption and desorption phenomena, there is no general agreement on the precise mechanism of ORR on Pt. We report here a more generalized and simplified scheme used to describe the pH dependence of the ORR on GDEs. The overall scheme, valid for both acid and alkaline electrolytes, is one previously proposed for the ORR on other metal surfaces [35, 36]:

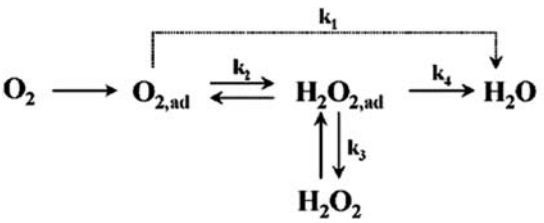

(3)

Based on this reaction scheme, three reaction pathways are possible. One is direct four-electron O_2 reduction to water (rate constant k_1) without intermediate formation of $H_2O_{2,ad}$. Second possible pathway is two-electron reduction to H_2O_2 (rate constant k_2), which can be either a final product (rate constant k_3), or further be reduced to water (k_4), i.e., the so-called serial four-electron pathway. Direct and serial four-electron pathways have the same final product, water molecules [37]. However, direct four-electron reduction requires dissociation of oxygen prior to the transfer of the first electron. The dissociation energy of O_2 is quite large (498 kJ mol^{-1}), which means that dissociation is energetically unfavorable unless the M–O bond is very strong (>250 kJ mol^{-1}). The more energetically favored path is the superoxo/peroxo path, with the transfer of the electron to the oxygen molecule. The dissociation energy of O_2^- and O_2^{2-} is much lower than that of O_2 (by 98.7 kJ mol^{-1}), resulting in a more facile reaction path without a strong M–O bond. The surface peroxide intermediate may or may not be further reduced to water

depending on the relative values of k_3 and k_4. Today there is general consensus that the addition of the first electron to O_2, and formation of the superoxide radical anion $\bullet O_2^-$ is the rate-determining step [35]:

$$O_2 + e^- \rightarrow O_2^-. \quad (4)$$

This reaction can proceed either as a reaction involving species in the solution (so-called outer sphere reaction), or as a reaction where reactant O_2 and product O_2^- are adsorbed on the electrode surface (inner sphere reaction). If a reaction (4) proceeds as an outer sphere reaction, equilibrium potential can be expressed as

$$E_{O_2/O_2^-} = E^0_{O_2/O_2^-} + 0.05916 \log \frac{P_{O_2}}{O_2^-}. \quad (5)$$

Yang and McCreery reported the standard equilibrium potential for reaction (4) as $E_{O_2/O_2^-} = -0.31$V versus standard hydrogen electrode (SHE) (pH 0) [38], corresponding to $\Delta G^\circ = 30$ kJ mol^{-1}. Because H^+ does not in reaction (4), the rate of this reaction step will not depend on the pH of electrolyte. The same conclusion holds if the reaction (4) proceeds via adsorbed intermediates ($O_{2,ad}$ and $O_{2,ad}{}^-$). The reaction is still pH independent, although the equilibrium potential is now shifted by the $-\Delta G_{ads}/F$, where ΔG_{ads} is adsorption energy of $O_{2,ad}{}^-$. The stronger the metal–$O_{2,ad}{}^-$ attractive interaction ($\Delta G_{ads} < 0$), the more the equilibrium potential for the reaction (4) is shifted positively, eventually becoming an exothermic process due to the O_2^- stabilization upon adsorption. Subsequent steps, i.e., protonation to form H_2O in four-electron reduction process or to form peroxide in two-electron process, are pH dependent. In acid solutions, overall reactions can be written as [39]:

$$O_2 + 4H^+ + 4e^- \rightarrow 2H_2O \quad (6)$$

$$O_2 + 2H^+ + 2e^- \rightarrow H_2O_2, \quad (7)$$

with corresponding expressions for equilibrium potentials in the form:

$$EO_2/H_2O_2 = 1.23 - 0.0591\text{pH} + 0.0147\log p_{O_2} \quad (8)$$

$$EO_2/H_2O_2 = 0.682 - 0.0591\text{pH} + 0.0295\log p_{O_2}/H_2O_2 \quad (9)$$

Since the rate-determining step, i.e. reaction (4), is pH independent, the reversible potential for the oxygen electroreduction should also be pH independent. If, however, we define the electrode potential using the reversible hydrogen electrode scale (i.e., taking into consideration the pH dependence of the overall process), then the overpotential for the oxygen electroreduction will be pH dependent and thus the polarization curves will shift with pH. This becomes obvious from Fig. 1, which is the modified form of the Pourbaix diagram. Instead of expressing the values of

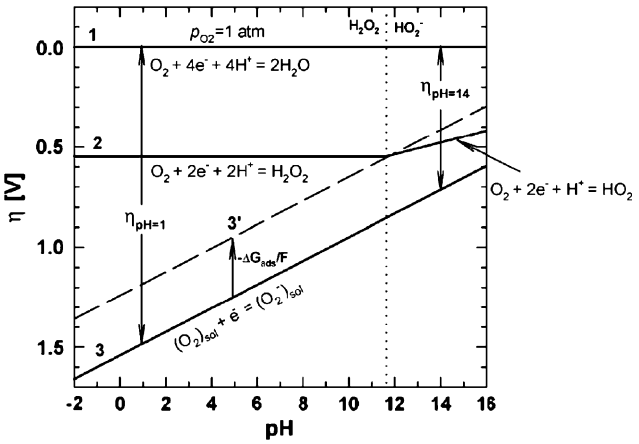

Fig. 1 Modified form of Pourbaix diagram. All potentials are expressed relative to the equilibrium potential for reaction (6). *Line 1*: pH dependence of equilibrium potential for reaction (6) ($p_{O2} = 1$ atm); *line 2*: pH dependence of equilibrium potential for reaction (7) ($\log(p_{O2}/(H_2O_2)) = 0$, $\log(p_{O2}/(HO_2^-)) = 0$); *line 3*: pH dependence of equilibrium potential for reaction (4) ($\log(p_{O2}/(O_2^-)) = 0$); *line 3′*: pH dependence of equilibrium potential for reaction (4) proceeding as an inner sphere reaction (ΔG_{ads} is adsorption free energy of $O_{2,ad}{}^-$; in this case, as illustration, ΔG_{ads} is about −30 kJ/mol)

equilibrium potentials for reactions (4–6) as a function of pH on the standard hydrogen electrode scale (pH 0), as is the case with conventional Pourbaix diagrams [39], equilibrium potentials here are expressed relative to the equilibrium potential for the four-electron O_2 reduction to water (*y*-axis is now oxygen electroreduction overpotential, η). Consequently, the pH-dependent process (6) now appears pH independent, and pH-independent process (4) now appears pH dependent. pH dependence/independence of process (7) is a little more complicated. Considering that H_2O_2 is a weak acid (p*K*a = 11.63), H_2O_2 is not stable in the solution at pH > 11.63, but dissociates into HO_2^- and H^+. As a result, O_2 reduction reaction to form HO_2^- proceeds as a process involving two electrons, but only one proton, leading to the different slope of d*E*/dpH (=−0.0296 V versus SHE/decade), compared with the four-electron O_2 reduction to H_2O, where d*E*/dpH = −0.0591 V versus SHE/decade, subsequently manifesting as a pH-dependent process on the overpotential scale. In the pH range where H_2O_2 is stable in the solution, pH dependence versus standard hydrogen electrode scale is the same as for the four-electron reduction; hence reaction appears pH independent versus the four-electron O_2 reduction equilibrium potential. Lines 1 and 2 in Fig. 1 define the overpotentials required for the four- and two-electron reduction of O_2. It was mentioned previously that the more energetically favored path for the four-electron O_2 reduction is through $H_2O_{2,ad}$ ($HO_{2,ad}{}^-$ at pH > 11.63) reaction intermediate (serial four-electron reduction). The equilibrium potential for H_2O_2 reduction to H_2O (not shown

in Fig. 1) is 1.77 V versus SHE, reflecting the highly exothermic nature of this process ($\Delta G^\circ = -340$ kJ/mol). For the four-electron reduction that proceeds via adsorbed $H_2O_{2,ad}$, equilibrium potential for the reaction (7) is shifted up (towards line 1) for the amount of adsorption energy of $H_2O_{2,ad}$, in analogy with the reaction (8) (and line 3 in Fig. 1). Based only on thermodynamical consideration, once formed $(H_2O_2)_{ad}$ should be readily reduced to H_2O. However, even though O–O bond in H_2O_2 is much weaker than in O_2 molecule, it still involves significant activation energy for its dissociation. Consequently, only substrates with relatively strong M–O bond can facilitate four-electron reduction of O_2 to H_2O, although the energy requirement in this case is not as stringent as for the direct four-electron reduction process. Since reaction (4) is rate-determining step, line 3 designate the minimum required overpotential for oxygen electroreduction as a function of pH. At pH 14 this overpotential is relatively small (even smaller if expressed as overpotential for the two-electron reduction process), indicating that no specific chemical interaction between surface and O_2 (or O_2^-) is required. This is the explanation why at high pH almost any electrically conducting material can be used to reduce oxygen to peroxide than at low overpotentials. However, at low pH, only surfaces with strong chemical interaction with O_2 (or O_2^-) (resulting in parallel shift of line 3 closer to lines 1 and 2) can reduce oxygen to peroxide at low overpotential, and even stronger interaction is required to reduce oxygen to water at low overpotential.

In this paper we have analyzed the effect of pH on the oxygen electroreduction on GDEs by comparing the ORR activity in 1 M NaOH and 2 M H_2SO_4 solutions (pH difference of approximately 12 units). However, in order to accelerate the oxygen reduction processes and to elevate catalytic activity, a high dispersion and the minimum amount of an expensive precious metal are necessary. The ideal support material should have the following characteristics: provide a high electrical conductivity, allow the reactant gas to get to the electrocatalyst easily, and also have adequate water-handling capability at the cathode where water is generated. To enhance the activity of ORRs, one strategy is to explore highly active catalysts with novel carbon material as a support. Carbon nanotubes (CNTs) have attracted much interest from both a fundamental and applied perspective since their discovery [40] and large-scale synthesis [41, 42].

The wide variety of pore structures and chemical functional groups on the surface of carbon supports affects the dispersion of Pt nanoparticles [43–45]. The structure of single-walled carbon nanotubes (SWNTs) is nearly perfect, even after functionalization, while other types of CNTs contain a significant concentration of structural defects in their walls. So catalysts supported on SWCNTs are studied in this research. Here, in order to improve the dispersion of platinum alloy catalysts deposited on SWCNTs, the surface of commercial SWCNT was functionalized with carboxyl functional groups.

The purpose of this study was to improve the catalytic activity of platinum by alloying with transition metals on oxygen reduction at cathode site, to compare the results in acidic and alkaline electrolyte, and to investigate the electrochemical and electrocatalytic characteristics of binary alloys in GDEs. Thus, Pt binary alloy catalysts were prepared with Pd. The alloy catalysts were characterized by X-ray diffraction and inductively coupled plasma atomic emission spectroscopy. The modified SWCNTs were supported alloy catalysts. We have focused on the preparation of Pt alloy catalysts with high total loading (50 wt.%). Then the modified SWCNTs supported alloy catalysts were used in catalyst layer of GDEs and characterized by various electrochemical techniques.

2 Experimental

2.1 Surface modification of SWCNTs

Previous work in our laboratory has shown that treatment of carbon with concentrated nitric acid increases its hydrophilicity by forming surface carboxylic acid functionality [43].

So, the surface of commercial SWCNT (Aldrich, OD: 1–2 nm, length 20–40 μm, purity 20–30%) was functionalized with carboxyl functional groups. For this purpose, commercial SWCNT and concentrated nitric acid were refluxed at 140°C for 7 h. It was then washed well with deionized water and dried to produce a modified catalyst.

2.2 Electrocatalyst preparation

To support Pt nanoparticles on the SWCNTs, we adopted the well-known impregnation method followed by liquid-phase borohydride. A mixture of modified SWCNTs and H_2PtCl_6 (Aldrich) was suspended by sonication in 40 mL deionized water. Subsequently, this Pt precursor was reduced and supported on SWCNTs simultaneously by $NaBH_4$ (Kanto Chemical) as the reducing agent and washed with deionized water several times. The filtrate was collected to determine an exact load by measuring the Pt residue. After drying, the SWCNTs supporting Pt nanoparticles were obtained. They were then dispersed in 25 mL deionized water and ultrasonically stirred for 10 min. Appropriate amounts of 0.1 M solution of transition-metal salts ($PdCl_2$) (Merck) were added to this suspension. The Pd precursor was reduced and supported on SWCNTs simultaneously by $NaBH_4$ (Kanto Chemical) as the reducing agent and washed with deionized

water several times. With the aim of studying the effect of composition on the performance of electrodes with Pt–Pd catalysts, i.e., which exhibited better performance, we prepared Pt–Pd alloys with different compositions (75:25 and 25:75 atomic ratios). Pd–Pt catalyst was prepared by consecutive deposition of Pt onto the supported Pd particles (Pt–Pd catalyst was prepared by consecutive deposition of Pd onto the supported Pt particles, with the reverse deposition manner for Pd–Pt catalyst). The atomic ratio of Pd–Pt was adjusted to 25:75. The obtained catalysts were characterized by recording powder X-ray diffraction (XRD) pattern on a Philips PW1800 X-ray diffractometer using CuK_{α} radiation operating at 40 kV and 30 mA. The analysis of atomic composition of the catalysts was performed with IRIS advantage inductively coupled plasma atomic emission spectroscopy (ICP-AES) system (Varian Austria).

2.3 Fabrication of gas diffusion electrode and electrochemical measurements

Porous GDEs were constructed according to a previously described procedure [18]. To prepare the polytetrafluoroethylene (PTFE)-bonded porous GDL, commercially available carbon Vulcan (XC-72R from ElectroChem Inc.) 70% and 30% polytetrafluoroethylene (PTFE) (from ElectroChem Inc.) emulsion was used and painted onto carbon paper TGP-H-0120 (Toray). The resulting composite structure was dried in air at 80–90°C for 1 h, followed by thermal treatment at 250°C for 30 min to remove the dispersion agent contained in the PTFE, and finally sintered in air at 340°C for 15 min. The PTFE is effective as a binder and it impacts hydrophobicity to the gas diffusion regime of the electrode.

To prepare the catalyst layer, a mixture comprised of a homogeneous suspension of Nafion, one of the as-received catalysts, and isopropyl alcohol as solvent was homogenized using a sonicator (Misonix Model S-3000) for 20 min. The prepared ink was painted on GDL. The resulting composite structure was dried in air at 25°C for 1 h and finally sintered in air at 140°C for 45 min.

Nafion and Pt loadings were 1 mg/cm^2 and 0.5 mg/cm^2 in the GDEs, respectively. The reduction of oxygen was investigated with the porous GDE (geometric exposed area of 1.3 cm^2) in 2 M H_2SO_4 solution and 1 M NaOH solution. These solutions were prepared from Merck products and very pure water (Millipore super-Q system). Linear sweep voltammetry (LSV) measurements were carried out at 298 K, in a conventional three-electrode cell, with O_2 flow rate of 50 mL min^{-1}. Cyclic voltammetry (CV) experiments were done under argon atmosphere. The GDEs were mounted in a Teflon holder containing a high pyrolytic graphite disk as a current collector (which had arrangement for oxygen feed from the back of the electrode). A large-area flat platinum electrode was used as the counterelectrode. An Ag/AgCl reference electrode was placed close to the working electrode surface. The electrochemical cell was connected to a potentiostat-galvanostat (Radiometer Model DEA332) digital electrochemical analyzer equipped with an IMT 102 electrochemical interface for the CV, chronoamperometry, and LSV measurements, and also to a computer-controlled 302 Autolab electrochemical system (EcoChemie, Utrecht, The Netherlands), driven with GPES and FRA software (EcoChemie), for electrochemical impedance spectroscopy (EIS) measurements. In the present work, an alternating-current (AC) potential amplitude of 5 mV in a frequency range from 10 mHz to 2.6 kHz was applied.

3 Results and discussion

3.1 Cyclic voltammetry (CV) study

Figure 2 shows a set of CV curves obtained with GDEs with Pt alloys catalysts (Table 1) in acidic electrolytes and alkaline electrolytes under argon reflux. The CV curves in the acidic electrolyte (Fig. 2a) reveal hydrogen adsorption/evolution currents indicative of the presence of Pt component on the surface of the bimetallic catalysts. Figure 2 also shows a single peak during cathodic sweep. This peak is normally assigned to the oxide-reduction profile of metals. The comparison of voltammograms in acidic (Fig. 2a) and alkaline (Fig. 2b) electrolytes for the same electrode shows that the charge for hydrogen desorption is negligible in alkaline electrolyte, in good agreement with Markovic et al.'s reports in their recent study [46]. It slightly increases when NaOH concentration decreases; this might be due to influence of OH^- concentration and, rather unlikely, to the very small traces of impurities left in NaOH.

As can be seen in Fig. 2, the second or third metal additions influence the oxide reduction potentials. In comparison with GDEs, there is an important observation for the oxide-reduction potential on the GDEs. The oxide reduction potential waves are highly dependent on the nature of the electrolyte. This wave for GDE3 is observed at about +450 mV in the acidic electrolyte (Fig. 2a), which is much more positive than −200 mV in the alkaline electrolyte (Fig. 2b). This may be related exclusively to the change in the mechanism and kinetics of the ORR as well as to the nature of electrolyte. Figure 2 also shows that the potential for oxide reduction in both acidic and alkaline electrolytes is highly dependent on the alloy's overall composition used in preparation of the GDEs. Increase of Pt in the catalysts leads to a more positive potential for oxide reduction in acidic and alkaline electrolytes. The loss of utilization in the alloy catalysts are explained by the loss

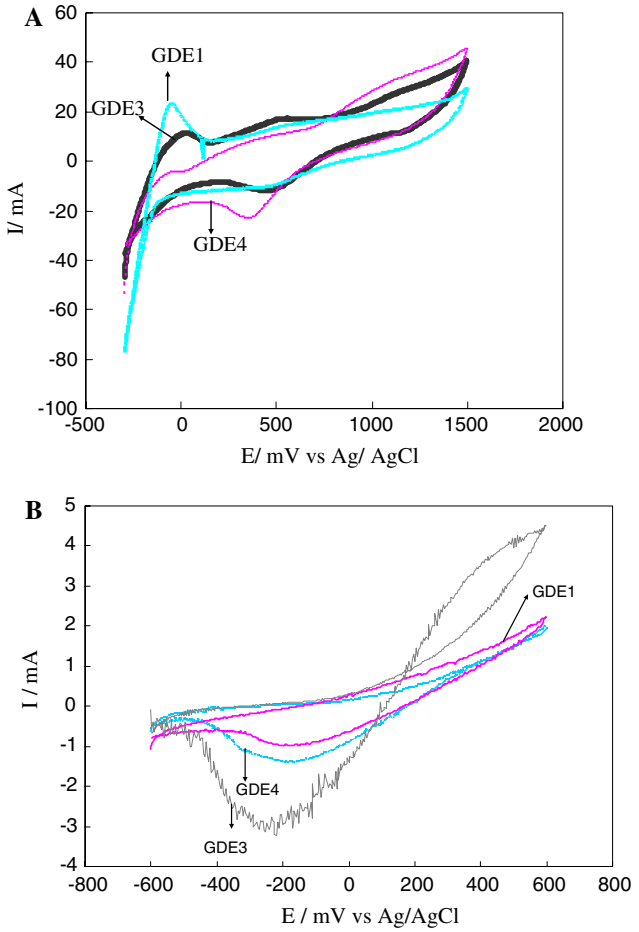

Fig. 2 The voltammograms of electrodes, each with Pt loading of 0.5 mg cm^{-2} and with Nafion loading of 1 mg cm^{-2} in the catalyst layer (scan rate; 50 mV s^{-1} temperature; 25°C), in acidic electrolyte (**a**, 2 M H_2SO_4) and in alkaline electrolyte (**b**, 1 M NaOH)

Table 1 The gas diffusion electrodes with various catalysts

Gas diffusion electrode	Catalyst used in catalyst layer
GDE1	Pt/CNT
GDE2	75:25 Pt Pd/CNT
GDE3	25:75 Pt Pd/CNT
GDE4	25:75 Pd Pt/CNT

of electrochemical surface area due in part to particle size and addition of the transition-metal ions. In the case of Pt alloys, the loss can be attributed to the decrease of surface Pt sites due to the substituted transition metals.

3.2 Determination of kinetic parameters

In order to obtain information about kinetic parameters of oxygen reduction reaction at fabricated GDEs, a Tafel plot was used. Its data were fitted using the following equation [47]:

$$E = E_0 - b\log(i) - iR, \tag{10}$$

where

$$E_0 = E_r + b\log(i_0). \tag{11}$$

In Eqs. 10 and 11, i_0 is the exchange current density for oxygen reduction, b is the Tafel slope, E_0 is the reversible potential for the oxygen electrode reaction, and R represents the resistance (predominantly the ohmic resistance of the electrolyte) responsible for the linear variation of potential versus current density. Equation 10 is valid up to the end of the linear region of the potential versus current density plot. At high current densities, the difference of the E versus i data from Eq. 10 is due to the rapidly increasing contribution of mass-transport overpotentials. The parameters E_0, b, and R were evaluated by nonlinear least-squares fitting of Eq. 10 to the experimental data. Using the R values, iR-corrected Tafel plots ($E + iR$ versus log i) were obtained. Variations of Tafel slopes with different catalysts in GDEs in both acidic and alkaline electrolytes are shown in Fig. 3. Compared with the Tafel slope values shown in Fig. 3, the Tafel slope values obtained for the GDEs in acidic electrolyte are smaller than in alkaline electrolyte, indicating better kinetics of ORR in acidic electrolyte in this study. The change of Tafel slope is related to the change in the mechanism and kinetics of ORR with the nature of electrolyte. Comparison of the GDEs with Pt–Pd as catalyst, with different compositions of Pt and Pd in the catalyst layer, it is observed that GDE2 presented the smallest Tafel slope value in both acidic and alkaline electrolytes. The strong dependence of the Tafel slopes on the bimetallic composition in both acidic and alkaline

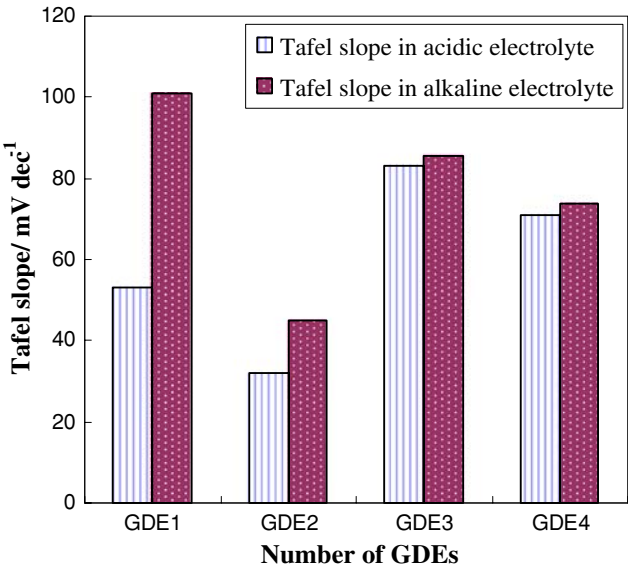

Fig. 3 Variation of Tafel slope with different catalysts used in preparation of the GDEs in acidic and alkaline electrolytes

electrolytes is evident from the exhibition of a minimum in GDE2. Calvo et al. reported [29] that 3:1 Pt–Pd (in this study used in preparation of GDE2) favors the reduction of OH with the surface compared with others, allowing weaker interaction of OH with the surface compared with other catalysts. According to their thermodynamic analysis, the best catalyst may be 3:1 Pt–Pd (in this study used in preparation of GDE2), which is almost as good as Pt for dissociating the O–O bond, and performs better than others for reduction of adsorbed O and OH. Their result is in good agreement with ours. Our results show that GDE2 presented smaller Tafel slope value than other GDEs and acts as the best GDE for ORR. Our results also indicated a promoting effect of the bimetallic catalyst in enhancing the ORR and that Pt–Pd specially with 3:1 atomic ratio (used to prepare GDE2) could be an economical candidate to replace Pt as a cathode fuel-cell catalyst. Remarkably, the Tafel slopes were also found to be strongly dependent on the bimetallic composition and on catalyst deposition manner on carbon nanotubes.

3.3 Chronoamperometry

Chronoamperometry was used to compare quantitatively the diffusivity of oxygen in GDEs according to Jiang et al. [48]:

$$i(t) = nFA(D/\pi t)^{1/2}C^*, \tag{12}$$

where i is the current (mA), n is the number of electrons, F is the Faraday constant (96485 C mol^{-1}), A is the surface area of the electrode (cm^2), D is the diffusion coefficient (cm^2 s^{-1}), t is the time (s), and C^* is the concentration of the reactant (mM).

$D^{1/2}C^*$ is defined as permittivity of oxygen at GDE. A Cottrell plot can be obtained from chronoamperometry (i versus $t^{-1/2}$) and the permittivity can be calculated from the slope of this plot. The variation of permittivity values of GDEs are given in Fig. 4. The GDEs consist of a distribution of pores with different radii (micro- and macropores) and therefore have different permittivity values. Uchida et al. [49] reported that the catalytic layer has two distinct pore-size distributions: the smaller pores (primary pores) are identified with the space in and between the primary pores in the agglomerate, and the larger pores (secondary pores) are located between the agglomerates. In Uchida's hypothesis, Nafion is localized only in the secondary pores and coats the agglomerates of electrocatalysts. By considering such a model, we can infer that the oxygen reduction reaction should be under the control of the following transport phenomena: (i) oxygen diffusion in the secondary and primary pores, (ii) oxygen diffusion in the Nafion, and (iii) proton transport in the Nafion. These phenomena are influenced by porosity that

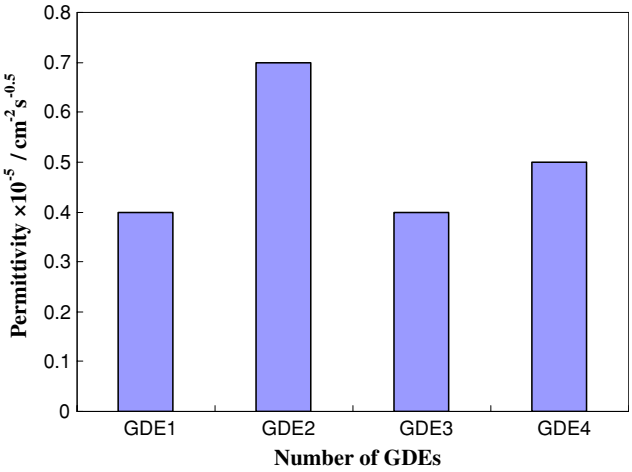

Fig. 4 Variation of the diffusion coefficient of the tested electrodes extracted from the chronoamperometry data

allows gas access to the active sites. In this study, the value of permittivity for GDE2 is more than for other GDEs. Comparing the GDEs with Pt–Pd as catalyst for different compositions of Pt and Pd in the catalyst layer it is observed that GDE2 presented the highest permittivity value. This result is consistent with the diffusion ability of oxygen into the reaction layer due to its high porosity. So, this combination of metals can create a catalyst layer with high porosity.

3.4 Characterization of alloy catalysts

Composition of the electrocatalysts was evaluated by ICP-AES analysis, and the results for all the catalysts were found to be nearly the same as the nominal values. Figure 5 shows X-ray diffraction patterns of the CNT-supported Pt alloy catalysts. The first peak, located at about 26.5° in all the XRD patterns, is associated with the CNT support. The other four peaks are characteristic of face-centered cubic (fcc) crystalline Pt (JCPDS-ICDD, Card No. 04-802), corresponding to the planes (1 1 1), (2 0 0), (2 2 0), and (3 1 1) at 2θ values of about 39.6°, 46.1°, 67.2°, and 81.8°, respectively, indicating that all the alloy catalysts are principally single-phase disordered structures (i.e., solid solutions). Since XRD is mass sensitive, a small fraction of much larger particles within the samples could produce the narrower diffraction peaks. Therefore, the broad diffraction peaks, as shown in Fig. 5, suggest that as-prepared Pt/CNT and 75:25 Pt–Pd/CNT exist in small particle sizes with a relative narrow particle-size distribution and in disordered form. Note in Fig. 5 that the PdO peak (JCPDS, card 46-1211) for 25:75 Pd–Pt/CNT is very broad and its crystalline size is considered to be very small. Indeed, if the reflection intensities of the other metals are low compared with those of platinum and/or the metals present in

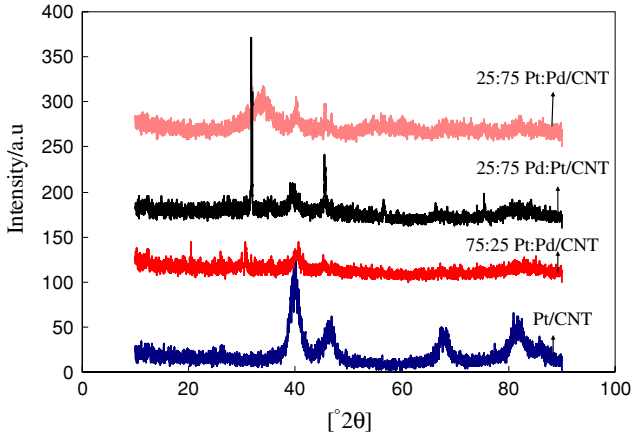

Fig. 5 X-ray diffraction patterns of the CNT-supported Pt alloy catalysts

amorphous compounds, they will not be detected in the diffractograms. A less likely possibility is that, in the preparation procedure, nanotube contaminants were covered by platinum to the point of not being detected, as shown for 25:75 Pt–Pd/CNT. The presence of palladium and cadmium incorporated as substituents in the platinum structure is noted through the shift of the Bragg angles with respect to the values for pure platinum. Compared with the same reflections in Pt, the diffraction peaks for the alloy catalysts are shifted very slightly to higher or lower 2θ values, probably indicating the formation of alloys involving Pd substituted into the fcc structure of Pt. The crystallite size of the catalysts was estimated from the XRD data using Scherrer's equation. For this purpose, the (2 2 0) reflection of the Pt face-centered cubic (fcc) structure around $2\theta = 67°$ was used. The particle size was calculated by Debye Scherrer equation [22]:

$$L = \frac{0.9\lambda_{\mathrm{CuK}}}{B_{2\theta}\cos\theta_{\max}}, \tag{13}$$

where L is the average particle size, λ_{CuK} is the X-ray wavelength, $B_{2\theta}$ is the full-width at half-maximum and $\theta_{\max}$ is the angle at peak maximum. The average particle sizes are provided in Table 2. For 75:25 Pt–Pd/CNT, the particle size was 29 nm. The large differences in particle size cannot be explained by the presence of other metals, as for 75:25 Pt–Pd/CNT the particle size was almost 29 nm. Larger differences were observed for 75:25 Pt–Pd/CNT and 25:75 Pt–Pd/CNT. The crystallite size of 75:25 Pt–Pd/CNT was 29 nm, while for 25:75 Pt–Pd/CNT it was much higher (58 nm), revealing the effect of various amounts of Pt and Pd in the binary catalysts.

Table 2 Comparison of average particle size from XRD

Gas diffusion electrode	Average particle size from XRD (nm)
GDE1	46
GDE2	29
GDE3	57
GDE4	35

4 Conclusions

The electrochemical properties of GDEs in acidic and alkaline media, using Pt-based binary and ternary alloy catalysts prepared by the borohydride reduction processes, have been investigated in the present research.

The pH effect on oxygen reduction reaction kinetics may be related exclusively to the change in the mechanism and kinetics of ORR. The results indicated that GDEs provide faster ORR kinetics in the acidic electrolyte than in the alkaline electrolyte. This indicates that electrochemical reduction of O_2 is influenced by the nature of the electrocatalysts and electrolyte medium.

GDE2 showed the smallest Tafel slope value compared with the other GDEs in acidic electrolyte. The concurrence of a maximized activity in GDE2 in both acidic and alkaline electrolytes suggests the operation of a remarkable synergistic effect.

Comparison of GDEs with Pt–Pd as catalyst for different compositions of Pt and Pd in the catalyst layer showed that GDE2 presented the smallest Tafel slope value in both acidic and alkaline electrolytes. This comparison indicates that the amount of transition metals in the catalyst may be one of the factors effective in determining the performance of the GDEs. Chronoamperometry showed that GDE2 presented the highest permittivity value. This is consistent with the diffusion ability of oxygen into the reaction layer due to its high porosity.

XRD studies on the electrocatalysts showed that the crystallite size of 75:25 Pt–Pd/CNT was 29 nm, while for 25:75 Pt–Pd/CNT it was much higher (58 nm). This reveals the effect of various amounts of Pt and Pd in the binary catalysts. These results suggest a change in crystallographic structure of the alloy electrocatalysts with respect to Pt.

References

1. El-Deab MS, Ohsaka T (2002) Electrochem Commun 4:288–294
2. Komai YJ (1998) Exp Biol 201:2359–2366
3. Andreasen A, Danscher G, Juhl S et al (1997) Neurosci Meth 72:15–27
4. Osborne PG, Li XF, Li YZ et al (2001) J Neurosci Res 63:224–230
5. Osborne PG (1997) Physiol Behav 61:485–492
6. Tarasevich MR, Sadkowski A, Yeagar EB (1983) In: Conway BE, Bockris J.O'M, Yeagar EB, White RE (Eds.), Comprehensive

treatise of electrochemistry, vol 7. Plenum Press, New York, p 301
7. Kinoshita K (1992) Electrochemical oxygen technology. Wiley, New York
8. Adzic RR (1998) In: Lipkowski J, Ross PN (eds) Electrocatalysis. Wiley-VCH, New York, p 197
9. Markovic NM, Ross PN Jr In: Wieckowski A (ed) Interfacial electrochemistry-theory, experiments and applications. Marcel Dekker, New York, p 821
10. Markovic NM, Schmidt TJ, Stamenkovic V et al (2001) Fuel Cells 1:105–116
11. Adzic RR, Markovic NM (1982) J Electroanal Chem 138:443–450
12. Adzic RR, Markovic NM, Vesovic VB (1984) J Electroanal Chem 165:105–112
13. Markovic NM, Adzic RR, Vesovic VB (1984) J Electroanal Chem 165:121–127
14. Anastasijevic NA, Dimitijevic ZM, Adzic RR (1986) Electrochim Acta 31:1125–1136
15. Taylor EJ, Vilambi NRK, Gelb A (1989) J Electrochem Soc 136:1939–1949
16. Paulus UA, Vokaun A, Scherer GG et al (2002) Electrochim Acta 47:3787–3799
17. Paulus UA, Vokaun A, Scherer GG et al (2002) J Phys Chem B 106:4181–4190
18. Mukerjee S, Srinivasan S, Soriaga MP (1995) J Phys Chem 99:4577–4589
19. Fernandez JL, Walsh DA, Bard AJ (2005) J Am Chem Soc 127:357–412
20. Balbuena PB, Altomare D, Agapito LA et al (2003) J Phys Chem B 107:13671–13680
21. Zhang J, Mo Y, Vukmirovic MB, Klie R et al (2004) J Phys Chem B 108:10955–10965
22. Zhang J, Vukmirovic MB, Xu Y et al (2005) Angew Chem Int Ed 44:2132–2143
23. Stamenkovic V, Schmidt TJ, Ross PN et al (2003) J Electroanal Chem 554–555:191–202
24. Shao MH, Sasaki K, Adzic RR (2006) J Am Chem Soc 128:3526–3532
25. Stamenkovic VR, Fowler B, Mun BS et al (2007) Science 315:493–497
26. Stamenkovic VR, Mun BS, Mayrhofer KJJ et al (2006) J Am Chem Soc 128:8813–8821
27. Wang Y, Balbuena PB (2005) J Phys Chem B 109:18902–18910
28. Sidik RA, Anderson AB (2002) J Electroanal Chem 528:69–76
29. Calvo SR, Balbuena PB (2007) Surf Sci 601:165–172
30. Yeager E (1986) J Mol Catal 38:5–11
31. Shimizu Y, Uemura K, Matsuda H et al (1990) J Electrochem Soc 137:3430–3438
32. Li N, Yan X, Zhang W et al (1998) J Power Sources 74:255–263
33. Arul Raj I, Vasu KI (1990) Int J Hydrogen Energy 15:751–760
34. Kannan AM, Shukla AK, Sathyanarayana S (1990) Bull Electrochem 6:273–281
35. Ross PN Jr (2003) Handbook of fuel cells: fundamentals, technology and applications. Wiley, p 465 (Chapter 31)
36. Markovic NM, Ross PN (2002) Surf Sci Rep 45:117–125
37. Adzic RR (1998) Electrocatalysis. Wiley–VCH Inc., New York, p 197
38. Yang H, McCreery RL (2000) J Electrochem Soc 147:3420–3428
39. Pourbaix M (1966) Atlas of electrochemical equilibria in aqueous solutions. Pergamon Press, London, pp 108–117
40. Iijima S (1991) Nature 354:56–62
41. Ebbesen TW, Ajayan PM (1992) Nature 358:220–227
42. Li WZ, Xie SS, Qian LX et al (1996) Science 274:1701–1705
43. Nozad Golikand A, Lohrasbi E, Ghannadi Maragheh M (2008) J Appl Electrochem 38:869–874
44. Li L, Wu G, Xu BQ (2006) Carbon 44:2973
45. Antonucci PL, Alderucci V, Giordano N et al (1994) J Appl Electrochem 24:58
46. Markovic NM, Gasteiger HA, Ross PN (1996) J Phys Chem 100:6715–6721
47. Sirinivasan S, E.Ticianelli A, Derouin CR (1988) J Power Sources 22:359–366
48. Jiang H, Zhu L, Moon KS et al (2007) Carbon 45:655–662
49. Uchida Y, Aoyama Y, Eda N et al (1995) J Electrochem Soc 142:4143–4150